Equation of state, refractive index and polarizability of compressed water to 7 GPa and 673 K

Cite as: J. Chem. Phys. **138**, 054505 (2013); https://doi.org/10.1063/1.4789359
Submitted: 01 December 2012 . Accepted: 10 January 2013 . Published Online: 05 February 2013

Carmen Sanchez-Valle, Davide Mantegazzi, Jay D. Bass, and Eric Reusser

Equation of state, refractive index and polarizability of compressed water to 7 GPa and 673 K

Carmen Sanchez-Valle,[1,a)] Davide Mantegazzi,[1] Jay D. Bass,[2] and Eric Reusser[1]
[1]*Institute for Geochemistry and Petrology, ETH Zurich, Switzerland*
[2]*Department of Geology, University of Illinois at Urbana-Champaign, Urbana, Illinois 61801, USA*

(Received 1 December 2012; accepted 10 January 2013; published online 5 February 2013)

The equation of state (EoS), refractive index n, and polarizability α of water have been determined up to 673 K and 7 GPa from acoustic velocity measurements conducted in a resistively heated diamond anvil cell using Brillouin scattering spectroscopy. Measured acoustic velocities compare favorably with previous experimental studies but they are lower than velocities calculated from the extrapolation of the IAPWS95 equation of state above 3 GPa at 673 K and deviations increase up to 6% at 7 GPa. Densities calculated from the velocity data were used to propose an empirical EoS suitable in the 0.6–7 GPa and 293–673 K range with a total estimated uncertainty of 0.5% or less. The density model and thermodynamic properties derived from the experimental EoS have been compared to several EoS proposed in the literature. The IAPWS95 EoS provides good agreement, although underestimates density by up to 1.2% at 7 GPa and 673 K and the thermodynamic properties deviate greatly (10%-20%) outside the estimated uncertainties above 4 GPa. The refractive index n of liquid water increases linearly with density and do not depend intrinsically on temperature. The polarizability decreases with pressure by less than 4% within the investigated P-T range, suggesting strong intermolecular interactions in H_2O that are consistent with the prevalence of the hydrogen bond network in the fluid. The results will allow the refinement of interaction potentials that consider polarization effects for a better understanding of solvent-solvent and ion-solvent interactions in aqueous fluids at high pressure and temperature conditions. [http://dx.doi.org/10.1063/1.4789359]

I. INTRODUCTION

Knowledge of the thermodynamic properties of water over a broad range of pressure and temperature conditions is important in a range of scientific disciplines, including Earth, planetary, and physical sciences.[1] In the Earth's interior, for instance, high pressure water-rich fluids mediate heat and mass transfer processes that ultimately shape its evolution and internal dynamics.[2] Significant efforts have been thus dedicated to determine accurate PVT equations of state (EoS) of water to predict its thermodynamic properties over a broad range of pressure (P) and temperature (T) conditions. However, the experimental data for the density of water are mainly restricted to pressures below 1 GPa[3–6] or to the extreme densities achieved above 200 GPa in shock wave experiments,[7,8] with very few experimental constraints at intermediate pressures.[9–11] The EoS for water at high pressure are thus based on empirical extrapolations of low pressure (<1 GPa) experimental data[12–17] and on molecular dynamic (MD) simulations using interaction potentials[18–20] whose accuracy is difficult to test due to the lack of high pressure experimental constraints. Among these EoS, the Saul and Wagner (1989)[15] and more recently the Wagner and Pruss (2002) (IAPWS95)[17] EoS, fitted to an extensive experimental dataset at low pressure, are considered the most accurate EoS at pressures below 1 GPa and temperatures up to 1273 K. However, the thermodynamic properties predicted by these EoS outside the calibration range deviate significantly when compared to experimental studies.[9] A more reliable extrapolation of the EoS of water beyond the experimental P-T range of calibration thus requires additional experimental constrains that will in turn allow for the refinement of inter-atomic potentials describing the evolution of atomic/molecular scale interactions in the fluid with pressure and temperature.

In the recent years, significant efforts have been dedicated to the development of interaction potentials for water,[21–23] with particular attention to those including polarization effects between water molecules. Polarization effects enhance intermolecular interaction and therefore, they have to be considered for an accurate description of the structural, dynamic, and thermodynamic properties of water at extreme high pressures and temperatures. The electronic polarization of water molecules is a measure of the relative tendency of its electron cloud to be distorted in an electrical field, which is manifested macroscopically by changes in the refractive index n. Direct measurements of the refractive index of water at high pressure and temperature will thus provide important information on the polarizability α of water molecules and on the microscopic scale interactions that are used for the refinement of interaction potentials. Although the refractive index and polarizability of room temperature water and ice phases have been accurately determined using first principle calculations[24] and reflectivity methods in the diamond

a)Author to whom correspondence should be addressed. Electronic mail: carmen.sanchez@erdw.ethz.ch.

anvil cell up to 120 GPa,[25,26] the polarizability of water molecules in high temperature compressed liquid water remain undetermined.

Here, we report Brillouin scattering measurements of the acoustic velocities of liquid water to 7 GPa and 673 K conducted using externally heated diamond anvil cells. The velocity data have been used to determine an empirical EoS of water valid in the measured P-T range and compare the derived thermodynamic properties to several EoS in the literature. Furthermore, the acoustic velocity data provide the first experimental constraints on the refractive index n and the polarizability α of water in the fluid phase over a broad range of pressure-temperature conditions.

II. EXPERIMENTAL METHODS

A. Diamond anvil cell techniques

Acoustic velocity measurements at room temperature were conducted in a three-pin Merrill Basset DAC modified for Brillouin scattering with large angular aperture. All high temperature measurements were conducted in a membrane-type diamond anvil cell[27] using a miniaturized platinum-wire resistive heater around the anvils and a ring-shaped Watlow® resistive heater surrounding the body of the cell. This configuration allows to minimize heat loss and thermal gradients across the cell, and to ensure thermal stability during the measurements as described in Refs. 28 and 29. The temperature was monitored simultaneously by two K-type chromel-alumel thermocouples attached to the diamond anvils very close to the compression chamber and by a K-type thermocouple attached to the external heater and calibrated against the temperature in the sample chamber before the experiments.

Sample chambers for measurements conducted between 293 and 473 K were formed from stainless-steel foils preindented to a final thickness of 60–80 μm and drilled with 185–200 μm holes in the center of the indentation. At higher temperature, and in order to avoid chemical reaction between the gasket and/or the pressure calibrants and the fluid, stainless-steel/platinum composite gaskets with two separated compression chambers were prepared following Datchi *et al.*[28] The larger compression chamber (~150–200 μm diameter) was loaded with ultra-pure water, whereas the second chamber (~60–70 μm) hosts the pressure calibrants embedded in paraffin oil. Pressure at temperature below 473 K was determined from the calibrated frequency shift of the R1 fluorescence line of ruby[30] after temperature correction.[31,32] At higher temperatures, as the ruby fluorescence lines broaden and become more difficult to resolve,[32,33] pressure was calibrated using the $^5D_0$–$^7F_0$ luminescence line of samarium-doped Sr-tetraborate (Sm^{2+}:SrB_4O_7).[32] Estimated uncertainties in pressure are about 0.02 GPa at 297 K, 0.05 GPa at 473 K, and 0.15 GPa at 673 K.

B. Brillouin scattering measurements

Brillouin scattering measurements were performed by using an Ar ion laser $\lambda_0 = 514.5$ nm as a light source and a six-pass tandem Fabry–Pérot interferometer equipped with a solid-state photon detector to analyze the frequency of the scattered light. All spectra were collected in symmetric/platelet scattering geometry in which the acoustic velocities are calculated using the following relationship:[34]

$$V_i = \frac{\lambda_0 \Delta \nu_i}{2 \sin(\theta_i/2)}, \quad (1)$$

where V_i is the compressional (V_P) phonon velocity, $\Delta\nu_i$ is the measured Brillouin shift, λ_0 is the laser wavelength ($\lambda_0 = 514.5$ nm), and θ is the external scattering angle, i.e., the angle between the incident and the scattered light outside the DAC. At high pressures, experiments were conducted either in 80° or 50° scattering to avoid vignetting effects.[35] To reduce geometric errors in the velocity measurements, the Brillouin system was calibrated using a MgO single-crystal standard. The accuracy in the measured acoustic velocities is within 0.5%–0.8% at high pressure although the precision of Brillouin frequency shifts is better than 0.4% at all investigated conditions.

Reference Brillouin spectra of water at ambient conditions were measured in a glass cuvette (1 mm length path) using a 90° scattering geometry. An additional set of measurements at room conditions were performed in glass cuvettes in 90°, 80°, and 50° scattering geometry at ETH Zurich using a solid-state laser ($\lambda_0 = 532.1$ nm), a Fabry–Perot interferometer, and a photomultiplier tube detector as described in detail in Ref. 36. Acoustic measurements were performed as a function of pressure along isotherms at 293, 373, 423, 473, 573, and 673 K. Measurements were extended up to the ice crystallization pressure with the exception of the 673 K isotherm, in which experiments were prematurely terminated due to gasket failure (Fig. 1). High pressure acoustic velocities were collected at room temperature in two independent runs, on both increasing and decreasing pressure, in the Merrill-Basset DAC using 80° scattering geometry. Redundant measurements were performed at selected pressures to check for internal consistency among the datasets. The reference velocities measured in glass cuvettes were crosschecked with measurements conducted inside the diamond anvil cell carefully

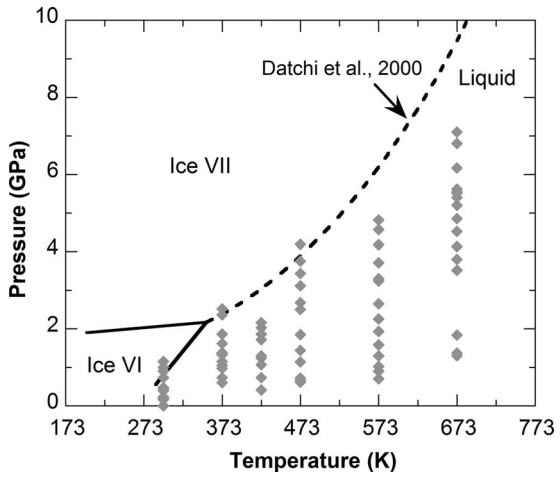

FIG. 1. Phase diagram of H_2O and P-T conditions investigated in this study. Brillouin measurements were collected along isotherms upon compression from the liquid phase up to the crystallization of ice. The dashed line corresponds to the melting curve of ice VII reported in Ref. 28.

closed without pressurization at the beginning of each run. All high temperature measurements were conducted in 50° scattering geometry and additional measurements at room temperature before the high temperature runs confirmed the accurate control of the scattering geometry. Typical acquisition times were less than 1 min/spectrum and at least two spectra were collected at each P-T point to increase the precision on the velocity determination.

III. RESULTS AND DISCUSSION

A. Sound velocities in H_2O at high P-T conditions

Figure 2 shows representative Brillouin spectra of H_2O collected at 293 K and 0.3 GPa and 673 K and 1.84 GPa in the externally heated diamond anvil cell. The strongest feature in the spectra corresponds to the compressional wave-velocities V_P in water in symmetric scattering. The lower intensity feature labeled as nV_P, where n is the refractive index of the fluid, corresponds to a backscattering signal (180° scattering) arising from light partially reflected from the output diamond anvil and acts as a secondary excitation source.

Acoustic velocities measured in water as a function of pressure up to 7 GPa along several isotherms from 293 to 673 K are reported in Figs. 3 and 4 and Table I. Figure 3 displays the acoustic velocities measured as a function of pressure at 293 K in several runs in both compression and decompression experiments, together with available literature data. Very good agreement is found between velocities measured inside and outside the diamond anvil cell and using different scattering geometries, demonstrating that the results are not affected by geometrical errors related to the DAC.[35] Overall, the Brillouin data at P < 0.2 GPa and above 0.4 GPa are in good agreement with literature data, including early ultrasonic,[37–39] optical interferometry,[40] the most recent measurements using light-scattering methods,[9,10] and acoustic velocities calculated from the EoS given in Refs. 15 and 17.

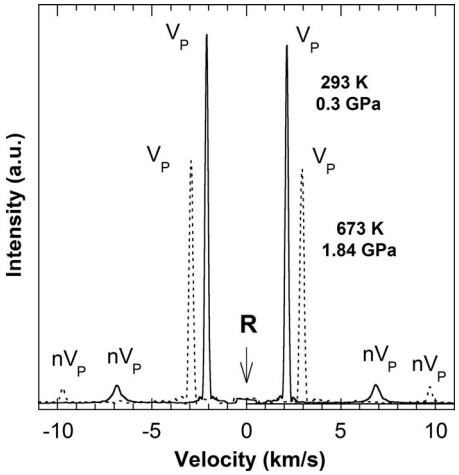

FIG. 2. Selected Brillouin spectra of H_2O collected in the diamond anvil cell at the indicated pressure and temperature conditions. The compressional wave velocity (V_P) and the backscattering (nV_P) signal are labeled. Typical acquisitions times are less than 1 min. Differences in V_P intensities are due to different laser output power. The Rayleigh elastic mode (R) has been suppressed for clarity.

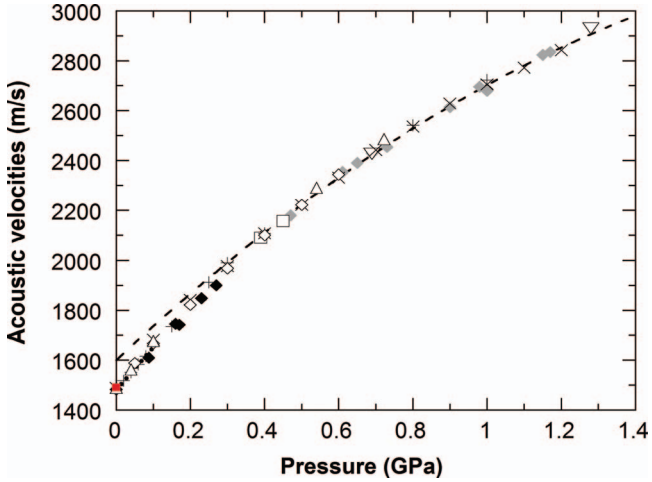

FIG. 3. Acoustic velocities (V_P) in H_2O as a function of pressure at 293 K. (red ■): Outside the DAC (this work); (black ♦, grey ◆): independent runs in 80° scattering geometry (this work); (□): 50° scattering geometry (this work); (●, Δ, ◊): ultrasonic measurements[37–39]; (×): optical interferometry[40]; (∇): impulsive stimulated scattering (ISS)[10]; (+): calculated from the equations of state of Refs. 15 and 17. Errors in the present Brillouin data do not exceed the size of the symbols (<0.5%). The dashed line is a guide for the eyes and shows changes in the pressure dependence of the acoustic velocities above 0.3-0.4 GPa, consistent with the liquid-liquid phases transition in water (LDW to HDW).

Between 0.2 and 0.4 GPa, our velocities are slightly lower than velocities determined using ultrasonic measurements but become comparable above 0.4 GPa. Subtle changes in the pressure dependence of the acoustic velocities of water have also been reported in previous Brillouin measurements[41] (data not available from the original reference) as well as on the high frequency acoustic velocities determined by X-ray inelastic scattering.[42] This anomaly is most likely associated to

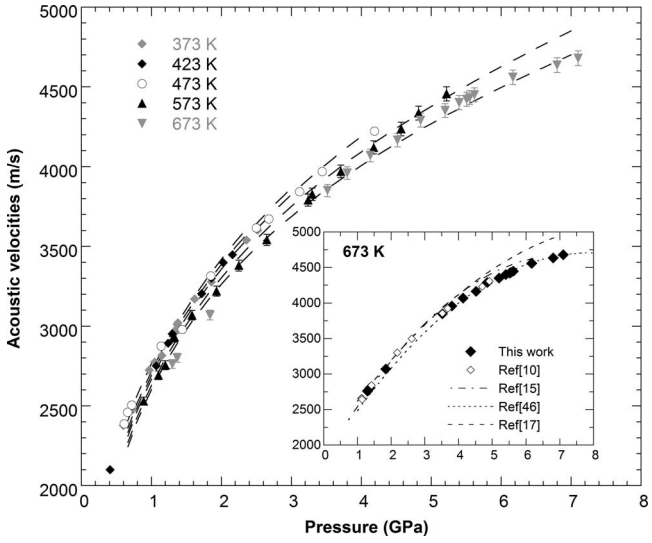

FIG. 4. Acoustic velocities (V_P) in water as a function of pressure from 373 to 673 K. Symbols are measured acoustic velocities in this work at 373 K (grey ◆); (○) 473 K; (▲) 573 K; and (grey ▼) 673 K. Dashed lines are acoustic velocities calculated from the equation of state given in Eq. (6). Inset: comparison between measured acoustic velocities in H_2O at 673 K [(♦) this work, (◊) Ref. 10, and (. . .) Ref. 46] and velocities calculated from the equations of state of Ref. 17 (- - - - -) and Ref. 15 (· — ·).

TABLE I. Measured acoustic velocities in H_2O to 7 GPa and 673 K. Velocities are determined with a precision of 0.5% below 473 K and with a precision of 0.8%-1% at higher temperature.

293 K		373 K		423 K		473 K		573 K		673 K	
P (GPa)	V_P (m/s)	P (GPa)	V_P (m/s)	P (GPa)	V_P (m/s)	P (GPa)	V_P (m/s)	P (GPa)	V_P (m/s)	P (GPa)	V_P (m/s)
0.00[a]	1483	0.60	2378	0.41	2100	0.61	2388	0.89	2530	1.30	2763
0.00[b]	1488	0.73	2475	0.73	2504	0.66	2461	1.10	2692	1.37	2802
0.00[c]	1479	0.97	2725	1.07	2752	0.72	2505	1.20	2755	1.84	3070
0.00[d]	1490	1.15	2816	1.24	2893	1.14	2874	1.33	2930	3.52	3850
0.09	1610	1.33	2970	1.72	3204	1.44	2979	1.58	3068	3.80	3960
0.16	1746	1.34	2960	1.86	3301	1.85	3316	1.93	3220	4.13	4070
0.17	1742	1.37	2994	2.03	3398	2.50	3615	2.25	3380	4.52	4166
0.23	1849	1.38	3002	2.16	3448	2.68	3671	2.65	3541	4.85	4291
0.27	1900	1.62	3150	2.75	3740	3.12	3843	3.24	3790	5.20	4352
0.39	2090	1.86	3278			3.44	3970	3.30	3827	5.40	4401
0.39	2090	2.36	3540			4.19	4222	3.71	3970	5.51	4422
0.39	2093	2.52	3602					4.18	4120	5.55	4432
0.41	2100							4.57	4236	5.62	4450
0.45	2157							4.82	4336	6.17	4560
0.45	2157									6.80	4636
0.47	2180									7.10	4680
0.60	2378										
0.61	2353										
0.61	2388										
0.65	2390										
0.66	2461										
0.69	2429										
1.00	2680										
1.00	2685										
0.90	2608										
0.73	2454										
0.98	2696										
1.15	2824										
1.17	2835										

[a]Glass cuvette (90° scattering).
[b]DAC (50° scattering).
[c]Glass cuvette (90° geometry, ETH Zurich).
[d]Glass cuvette (50° geometry, ETH Zurich).

the low-density (LDW) to high-density (HDW) transition in water,[43] as also identified by previous Raman[43] and theoretical studies[44,45] in this pressure interval. This phase transition involves the reorganization of the hydrogen bonding network of water and the collapse of the second coordination shell onto the first shell due to broken H bonds, as shown by neutron diffractions studies.[43] The absence of anomalies in the ultrasonic measurements thus suggests that the higher frequency measurements by Brillouin and X-ray scattering are more sensitive to the dynamical and structural properties of water, most likely due to the strength of the relaxation.[42]

The evolution of the acoustic velocities with pressure and temperature is shown in Fig. 4. Acoustic velocities increase monotonously with pressure along each isotherm but the temperature dependence remains moderate compared to the pressure dependence at the investigated conditions. Note that although the LDW to HDW transition also occurs in high temperature water,[44] the nonlinearity in the pressure dependence of the velocities is much more subtle at high temperature.[41] In our study, the lower data coverage at high temperature does not allow us to identify anomalies in the pressure dependence of the acoustic velocities (Fig. 4). The inset in Fig. 4 compares the acoustic velocities in water determined at 673 K in this work with available experimental data[10,46] and velocities derived from the EoS of Refs. 15 and 17. The present measurements reproduce very well previous impulsive stimulated scattering (ISS) and Brillouin measurements performed in the diamond anvil cell using the double-hole gasketing technique,[10,28,46] with maximum deviation of 0.5% below 3 GPa, that is within overall experimental errors. Although the acoustic velocities derived from the EoS of Refs. 15 and 17 compare well with experimental results within errors below 3 GPa, a systematic deviation toward higher velocities is observed above this pressure as found previously.[10] At 7 GPa and 673 K, the velocities predicted by the IAPWS95 EoS[17] are larger than the experimental values by 6%.

B. Equation of state of H_2O to 7 GPa and 673 K

The experimentally determined acoustic velocities, V_P, in the fluid are related to the density of the fluid through the

thermodynamic relations:

$$\left(\frac{\partial \rho}{\partial \mathrm{P}}\right)_{\mathrm{T}} = \frac{1}{\mathrm{V_P^2}} + \frac{\mathrm{T}\cdot\alpha_{\mathrm{P}}^2}{\mathrm{C_P}}, \tag{2}$$

$$\alpha_{\mathrm{P}} = -\frac{1}{\rho}\cdot\left(\frac{\partial \rho}{\partial \mathrm{T}}\right)_{\mathrm{P}}, \tag{3}$$

$$\left(\frac{\partial C_P}{\partial \mathrm{P}}\right)_{\mathrm{T}} = -\mathrm{T}\cdot\left(\frac{\partial^2 \mathrm{v}}{\partial \mathrm{T}^2}\right)_{\mathrm{P}} = -\frac{\mathrm{T}}{\rho}\cdot\left[\alpha_P^2 + \left(\frac{\partial \alpha_P}{\partial \mathrm{T}}\right)_{\mathrm{P}}\right], \tag{4}$$

where V_P is the measured acoustic velocity (m/s), ρ is the density (kg/m^3), α_P is the coefficient of thermal expansion (K^{-1}), C_P is the isobaric specific heat capacity (Jkg^{-1}K^{-1}), and v is the specific volume (m^3/kg). The measured acoustic velocities were inverted using the iterative procedure outlined in Refs. 10, 29, and 47 to obtain the density of water at high pressure-temperature conditions. The integration of these equations requires the sound velocities as a function of pressure and temperature, and the densities and specific heat capacities at one reference pressure. In the first step, the acoustic velocities are integrated neglecting the isothermal-adiabatic correction ($T\cdot\alpha^2/C_P$). The resulting density is used to calculate a first approximation for α_P and C_P (Eqs. (3) and (4)) that are further used in the next iteration of Eq. (2). This process is reiterated until convergence. The inversion was first tested using the acoustic velocity data derived from the IAPWS95 EoS[17] and data reported in previous Brillouin scattering studies.[9,10] The inversion reproduces the ρ, α, and C_P with a maximal relative deviation of 0.3%–0.4%.

For the integration, the experimental acoustic velocities measured above 373 K and 1 GPa were interpolated to produce a mesh of acoustic velocity values in the pressure-temperature space using the following analytical expression:

$$\mathrm{V_{P,\,this\ work}}(P,T) = \mathrm{V_{P,IAPWS\text{-}95}}(P,T)/(1-(-8.1246\cdot10^{-3}\cdot P + 4.1926\cdot10^{-3})), \tag{5}$$

where $V_{P,IAPWS\text{-}95}(P,T)$ are the acoustic velocities calculated from the IAPWS95 EoS,[17] T is the temperature in Kelvin and P is the pressure in GPa. The room temperature and low pressure (<1 GPa) data were excluded to optimize the fit in the high pressure-high temperature region. Equation (5) reproduces the experimental V_P data with a maximal deviation of 0.5% at 673 K. The integration of Eq. (2) started at 1 GPa at each isotherm from 373 to 673 K using initial values of density ρ and isobaric heat capacity C_P at 1 GPa at the corresponding temperature from the IAPWS95 EoS.[17] The inversion procedure allows retrieving the densities with uncertainties smaller than 0.5% as estimated from the propagation of experimental errors (Fig. 5).[47]

The inverted densities were combined with data at pressure below 1 GPa and 373 K from Ref. 17 to generate a best-fit empirical equation of state of the type

$$\rho(T,P,x) = a(T) + b(P) + c(T,P) \tag{6}$$

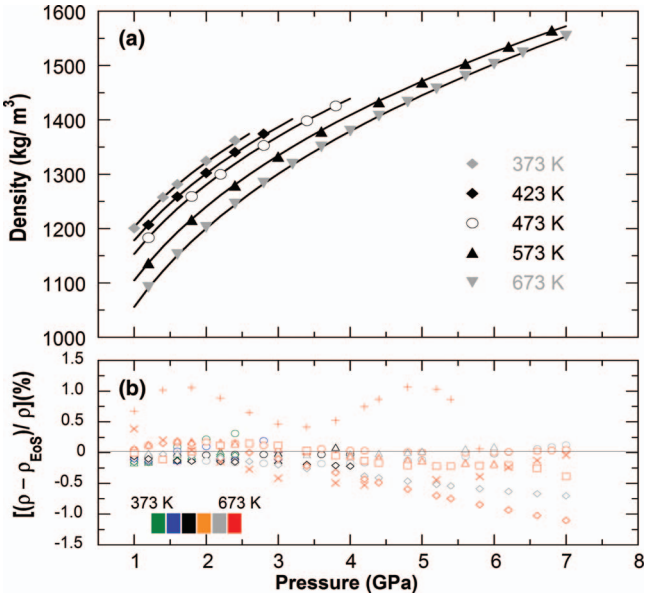

FIG. 5. (a) Density of H_2O as a function of pressure along isotherms. Symbols denote density determined through inversion of the acoustic velocity data and the solid lines are densities calculated using the best-fit EoS given in Eq. (6) with the best fit parameters listed in Table II. Errors in the inverted densities are within the symbol size (0.5%). (b) Comparison between densities determined from Eq. (6) with data from selected equations of state for H_2O at various temperatures: (○) inverted densities (this work); (×) Ref. 14; (+) Ref. 11; (◊) Ref. 17; (□) Ref. 20; (Δ) Refs. 9 and 10. Deviations of density datasets with respect to the equation of state obtained in this study are reported as $[(\rho - \rho_{EoS})/\rho](\%)$, where ρ denotes the datasets listed above and ρ_{EoS} refers to Eq. (6).

with

$$a(T) = a_1 + a_2\cdot T + a_3\cdot T^2,$$
$$b(P) = b_1\cdot\sqrt{P} + b_2\cdot P,$$
$$c(T,P) = c_1\cdot T\cdot P + c_2\cdot T\cdot\ln(P),$$

where T is the temperature in Kelvin and P is the pressure in Pascal. The best-fit coefficients a_i, b_i, and c_i are tabulated in Table II. The proposed equation of state (Eq. (6)) reproduces the inverted densities with an average deviation of 0.3% (Fig. 5) and the experimental acoustic velocities with a maximal misfit of 1.2% at 673 K (Fig. 4). This indicates that our equation of state is fairly satisfactory and that can be confidently used to predict the density and properties of water in the 0.6–7 GPa and 293–673 K range.

TABLE II. Best-fit parameters for Eq. (6).

Parameters	
a_1	1.148187×10^{3}
a_2	−2.540804
a_3	2.917138×10^{-5}
b_1	8.507742×10^{-3}
b_2	-2.412079×10^{-8}
c_1	1.811854×10^{-11}
c_2	9.660446×10^{-2}

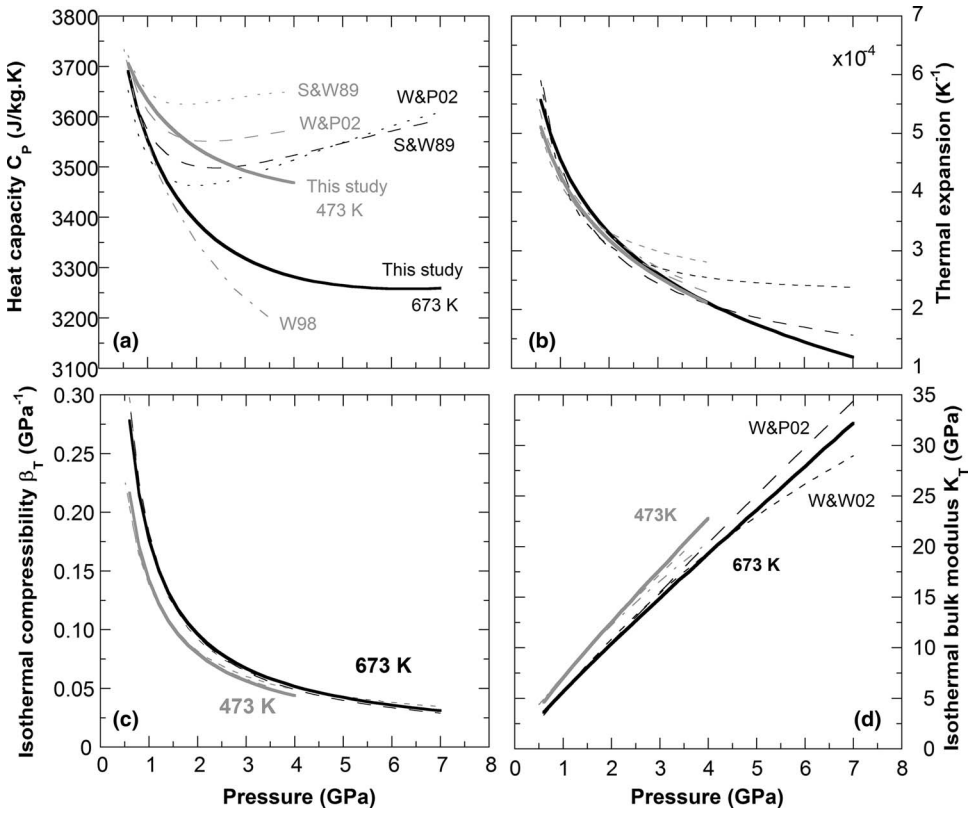

FIG. 6. Pressure dependence of the thermodynamic properties at H_2O along isotherms at 473 (solid grey lines) and 673 K (solid black lines) calculated from the best-fit EoS proposed in Eq. (6): (a) Thermal expansion coefficient α_P; (b) isobaric heat capacity C_P; (c) isothermal compressibility β_T; and (d) isothermal bulk modulus K_T. Dashed, short dashed, and dotted-dashed lines denote properties derived from the EoS reported in Ref. 17 (W&P02), Ref. 15 (S&W89), and Ref. 9 (W98), respectively.

C. Thermodynamic properties of H_2O and comparison with previous studies

Figure 5 compares the density of water calculated along various isotherms from Eq. (6) with literature data, including densities from previous light-scattering measurements,[9,10] empirical EoS,[12,15,17] and the most recent EoS derived from MD simulations.[20] Data derived from other theoretical studies[18,19] have been excluded from the comparison because their accuracy to predict the density of water has been discussed previously.[9–11] Densities obtained from the present Brillouin study are in fairly good agreement with results from ISS measurements[9,10] and theoretical EoS,[19] with differences smaller than 0.4%–0.5% in the investigated P-T range. However, H_2O is denser than predicted by the extrapolation of the IAPWS-95 above 3 GPa and the deviation increases with temperature, reaching up to 1.2% at 7 GPa and 673 K. It is also worth noting that the empirical EoS of Ref. 12 displays a non-systematic deviation on density, reaching differences of up to 1.3% at 5 GPa.

Using the EoS (Eq. (6)), we calculate the thermodynamic properties of water in the 0.6–7 GPa range up to 673 K, including the isobaric thermal expansion coefficient (α_P), specific heat capacity (C_P) as well as the isothermal and adiabatic compressibility (β_T and β_S) and bulk modulus (K_T and K_S). According to error propagation calculations, estimated maximal uncertainties on the coefficient of thermal expansion α_P and the isobaric heat capacity C_P are about 2%–3%, whereas larger uncertainties of 4% and 6% are estimated for the adiabatic and isothermal bulk modulus (K_S and K_T) and compressibility (β_S and β_T), respectively. The results are tabulated in supplementary Table AI[48] and plotted at selected temperatures in Fig. 6, together with data from commonly used EoS[15,17] and previous experimental studies.[9] The figure illustrates that although densities predicted from the present work and the IAPSW95 EoS are in relatively good agreement (<1.2%), the derived thermodynamic properties differ significantly at high pressure. This is most noticeable in the isothermal evolution with pressure of the heat capacity C_P at 673 K at pressures above 2 GPa. The C_P derived from this study continuously decreases with pressure until it approaches a constant value above 4 GPa, whereas that derived from the IAPWS95 EoS[17] and Saul and Wagner's EoS[15] slightly increases above 2 GPa. These two EoS thus overestimate the C_P by about 10% at 673 K and 7 GPa. A similar behavior is observed for the thermal expansion, although differences with the IAPWS95 EoS[17] are most noticeable at pressures above 4 GPa at 673 K, reaching values of up to 20% at 7 GPa. These differences are well outside the present uncertainties, indicating that the accuracy of the IAPWS95 EoS[17] to predict the thermodynamic properties of water rapidly decreases when extrapolated above 4 GPa. The new experimental constrains on the EoS of water derived from this study thus may allow further refinement of the theoretical approaches to provide a more reliable extrapolation of the properties of water over a broader range of P-T conditions.

TABLE III. Refractive index n and polarizability α of water to 673 K and 5.6 GPa. The estimated error in n and α are 1% and 1.5%, respectively.

293 K			373 K			473 K			573 K			673 K		
P	n	α (10^{-30} m^3)	P	n	α (10^{-30} m^3)	P	n	α (10^{-30} m^3)	P	n	α (10^{-30} m^3)	P	n	α (10^{-30} m^3)
0.00[a]	1.332	1.455	0.60	1.370	1.428	0.61	1.359	1.458	0.89	1.358	1.446	1.30	1.364	1.438
0.03	1.327	1.428	0.73	1.379	1.426	0.66	1.364	1.461	1.10	1.369	1.437	1.37	1.363	1.420
0.08	1.332	1.419	0.97	1.396	1.432	0.72	1.366	1.452	1.20	1.375	1.437	1.84	1.399	1.462
0.09	1.339	1.441	1.05	1.394	1.411	1.14	1.386	1.427	1.33	1.385	1.447	3.80	1.451	1.409
0.16	1.358	1.478	1.15	1.395	1.398	1.44	1.398	1.416	1.58	1.393	1.431	4.13	1.458	1.403
0.27	1.359	1.435	1.33	1.400	1.386	1.85	1.416	1.416	2.25	1.422	1.433	4.52	1.471	1.410
0.39	1.367	1.423	1.34	1.401	1.388				2.65	1.422	1.391	4.85	1.476	1.402
0.45	1.371	1.419	1.37	1.402	1.387							5.51	1.492	1.404
0.47	1.378	1.437	1.38	1.412	1.416							5.55	1.478	1.368
0.61	1.408	1.496										5.62	1.489	1.391
0.65	1.385	1.412												
0.69	1.393	1.429												
0.98	1.412	1.433												
1.00	1.420	1.454												
1.17	1.434	1.468												
0.00[b]	1.338	1.467												

[a]Measured with laser wavelength $\lambda_0 = 514.5$ nm.
[b]Measured with laser wavelength $\lambda_0 = 532.1$ nm.

D. Refractive index *n* and polarizability α of H_2O

The acoustic velocities measured in water simultaneously in platelet (90°, 80°, and 50°) and backscattering (180°) scattering geometries (Fig. 2) were used to determine the refractive index n of water from room pressure 5.6 GPa and 293 to 673 K. In an isotropic medium, the measured Brillouin shifts in platelet ($\Delta\nu_{\theta_i}$) and 180 ($\Delta\nu_{180°}$) scattering geometries are related to the refractive index n through the relationship:

$$n = \left(\frac{\Delta\nu_{180°}}{\Delta\nu_{\theta_i}}\right)\sin\left(\frac{\theta_i}{2}\right), \tag{7}$$

where θ_i is the scattering angle in platelet geometry (90°, 80°, or 50°) (Fig. 2). The calculated refractive index n for water is listed in Table III and displayed as a function of pressure at various temperatures from 293 to 673 K in Fig. 7.

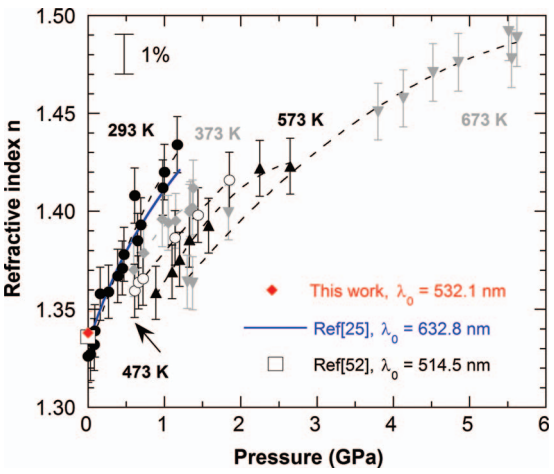

FIG. 7. Refractive index n of H_2O measured at $\lambda_0 = 514.5$ nm as a function of pressure along various isotherms from 293 to 673 K. (●) 293 K; (grey ◆) 373 K; (○) 473 K; (black ⧫) 573 K; (grey ▼) 673 K. Dashed lines are guides for the eyes.

The refractive index smoothly increases with pressure along an isotherm but decreases with increasing temperature, as observed for other molecular liquids such as CO_2, NH_3, and CH_4.[49–51] The refractive index of H_2O determined in this study at room conditions for the 514.5 nm wavelength, $n = 1.332 \pm 0.002$, is consistent with the value of 1.336 reported in Ref. 52 within experimental errors. The room temperature data are also in agreement with measurements using the interferometry method in the diamond anvil cell with a laser wavelength of 632.8 nm.[25] This is consistent with the weak dispersion in the refractive index of H_2O previously reported.[25,53] In Fig. 8, the refractive index n of water is reported as a function of density, together with previous room temperature data.[25,52] The refractive index n increases linearly with density and a fit to the Gladstone-Dale relation,[54] $n = a + b \cdot \rho$, provides best-fit coefficients of a = 1.00 ± 0.01 and b = 3.3 × 10^{-4} ± 8 × 10^{-5} m^3/kg. The coefficients compare well with those reported for room temperature liquid water data,[25] indicating that temperature affects n only insofar as temperature affects density. This indicates that the linear relationship can be confidently used at higher pressures and temperatures to determine the refractive index of liquid water.

The polarizability α of water molecules was determined from the refractive index n using the Lorentz-Lorenz relation:

$$\left(\frac{n^2-1}{n^2+2}\right) = \frac{4}{3}\pi\left(\frac{\rho N_A}{M}\right)\alpha, \tag{8}$$

where N_A is the Avogadro's number, 6.023 × 10^{23}, and ρ and M are the density and molar mass (M = 18.01528 g/mol) of water, respectively. Calculated polarizabilities using our measured refractive index and inverted densities are reported in Table III and shown as a function of density in Fig. 8. At room conditions, we find a value of 1.455(20) × 10^{-30} m^3 that compares favorably with the average polarizability reported for room P-T water by first-principle calculations.[24] We note a

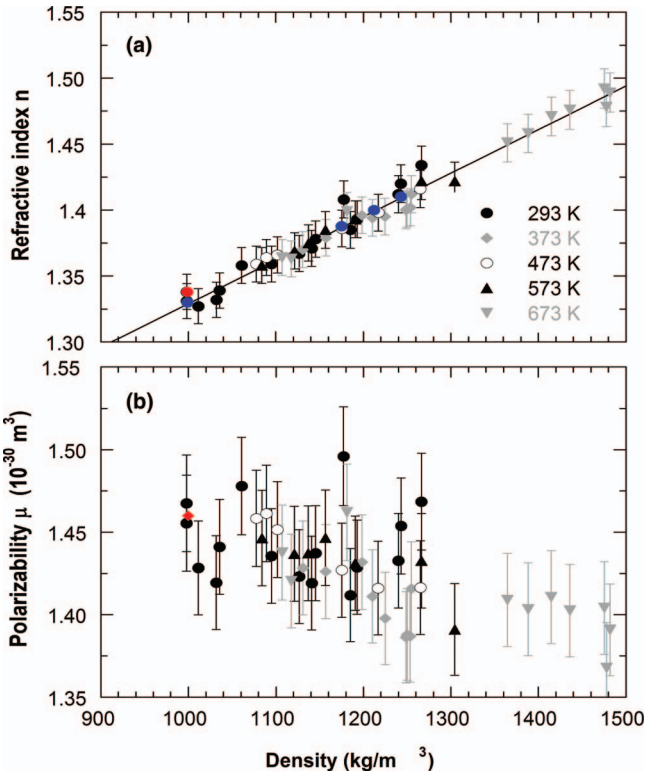

FIG. 8. (a) Refractive index n and (b) polarizability α of H_2O as a function of density at $0 < P < 5.6$ GPa and $293 < T < 673$ K. Red and blue dots in (a) are experimental data from Refs. 52 and 25, respectively. The polarizability α was calculated from n and $\rho(P,T)$ using the Lorentz-Lorenz relation [Eq. (8)]. The red diamond shows the polarizability determined at room P-T in Ref. 24 from first principle calculations. The solid line in (a) is a fit to data using the Gladstone-Dale relation,[54] $n = a + b.\rho$, with best-fit coefficients $a = 1.00 \pm 0.01$ and $b = 3.3 \times 10^{-4} \pm 8 \times 10^{-5}$ m^3/kg.

very subtle decrease of the polarizability of individual H_2O molecules with density, reaching a value of 1.391×10^{-30} m^3 at a density of 1.489 g/cm^3 (5.92 GPa–673 K). The decrease in the polarizability upon compression may be explained by the reduction in the distortion of the electron cloud of the individual water molecules, leading in turn to a decrease of the intermolecular interactions with neighboring molecules. The moderate change by ~4% in the polarizability of water in the investigated density range contrasts with the evolution observed in other molecular systems such as H_2,[55] where the polarizability decreases by 12% when density changes by only 0.2 g/cm^3. This observation indicates that the interactions between water molecules remain relatively strong, in agreement with the prevalence of the hydrogen bond network in hot compressed water in the investigated P-T range.[56]

The dataset reported in Fig. 8 and Table III is, to the best of our knowledge, the first determination of the refractive index and polarizability of liquid water at high pressure-temperature conditions. It is expected that the present results will assist in the validation of computational studies of the properties of hot compressed water and on the refinement of interaction potentials which include polarization effects.[21–23] This will in turn contribute to better the understanding of ion solvation processes and solvent-solute interactions in aqueous fluids at high pressure and temperature conditions.

IV. CONCLUSIONS

Acoustic velocity measurements in water have been performed up to 7 GPa and 673 K in externally heated diamond anvil cells using Brillouin scattering spectroscopy. The measurements compare favorably with previous experimental studies but deviations of up to 2% from velocities calculated from commonly used EoS[15,17] are observed at pressure above 3 GPa at 673 K. The acoustic velocity data were used to determine the density of water and an empirical EoS suitable in the 0.6–7 GPa and 293–673 K and an estimated total uncertainty of 0.5% has been proposed. The density model and thermodynamic properties derived from the experimental EoS have been compared to several EoS proposed in the literature. The IAPWS95 EoS provides the best agreement, although it underestimates density by up to 1.2% at 7 GPa and 673 K and the thermodynamic properties deviate at pressure above 4 GPa.

The present Brillouin measurements also provide first constraints on the refractive index n and polarizability α of liquid water at high pressure and temperature conditions. The refractive index increases linearly with pressure and do not depend intrinsically on temperature. The polarizability of water at room conditions is in good agreement with values reported from first principles and decreases with pressure by less than 4% within the investigated P-T range. This observation indicates that interactions between water molecules remain strong, in agreement with the prevalence of the hydrogen bond network in hot compressed water in the investigated P-T range. The results reported here will assist in the refinement of interaction potentials which include polarization effects, contributing to advance our understanding of solvent-solvent and ion-solvent interaction in aqueous fluids at high pressure and temperature conditions.

ACKNOWLEDGMENTS

We thank A. G. Kalinichev for providing the code for solving the Saul and Wagner (1989) EoS and an anonymous reviewer for comments that helped to improve the paper. The associate editor Dr. Edward W. Castner is acknowledged for efficient editorial handling. This work was partially supported by ETH Zurich though the ETHIIRA Grant No. ETH-30 08-2 to C.S.V. and by Grant Nos. DOE DE-FG02-08ER and NSF EAR 0738871 to J.D.B.

[1]H. Weingartner and E. U. Franck, Angew. Chem., Int. Ed. Engl. **44**, 2672 (2005).
[2]C. E. Manning, Earth Planet. Sci. Lett. **223**, 1 (2004).
[3]G. S. Kell and E. Whalley, J. Chem. Phys. **62**, 3496 (1975).
[4]G. S. Kell, G. E. McLaurin, and E. Whalley, Proc. R. Soc. London, Ser. A **360**, 389 (1978).
[5]C. W. Burnham, J. R. Holloway, and N. F. Davies, Am. J. Sci. **256-A**, 70 (1969).
[6]N. Rosner and J. Straub, in *Water and Steam*, edited by J. Straub and K. Scheffler (Pergamon, New York, 1980).
[7]A. Mitchell and W. Nellis, J. Chem. Phys. **76**, 6273 (1982).
[8]M. D. Knudson *et al.*, Phys. Rev. Lett. **108**, 091102 (2012).
[9]S. Wiryana, L. J. Slutsky, and J. M. Brown, Earth Planet. Sci. Lett. **163**, 123 (1998).
[10]E. H. Abramson and J. M. Brown, Geochim. Cosmochim. Acta **68**, 1827 (2004).

[11]A. C. Withers, S. C. Kohn, R. A. Brooker, and B. J. Wood, Geochim. Cosmochim. Acta **64**, 1051 (2000).
[12]H. Halbach and D. Chatterjee, Contrib. Mineral. Petrol. **79**, 337 (1982).
[13]L. Haar, J. S. Gallagher, and G. S. Kell, *NBS/NRC Steam tables* (Hemisphere, Bristol, PA 1984).
[14]S. K. Saxena and Y. Fei, Geochim. Cosmochim. Acta **51**, 783 (1987).
[15]A. Saul and W. Wagner, J. Phys. Chem. Ref. Data **18**, 1537 (1989).
[16]K. S. Pitzer and S. M. Sterner, J. Chem. Phys. **101**, 3111 (1994).
[17]W. Wagner and A. Pruß, J. Phys. Chem. Ref. Data **31**, 387 (2002).
[18]A. Belonoshko and S. K. Saxena, Geochim. Cosmochim. Acta **55**, 381 (1991).
[19]J. Brodholt and B. Wood, J. Geophys. Res. **98**(B1), 519, doi:10.1029/92JB01407 (1993).
[20]Z. G. Zhang and Z. H. Duan, Phys. Earth Planet. Inter. **149**, 335 (2005).
[21]H. J. C. Berendsen, J. R. Grigerat, and T. P. Straatsma, J. Phys. Chem. **91**, 6269 (1987).
[22]B. Guillot and Y. Guissani, J. Chem. Phys. **114**, 6720 (2001).
[23]A. A. Chialvo and J. Horita, J. Chem. Phys. **133**, 074504 (2010).
[24]M. Salanne *et al.*, J. Phys.: Condens. Matter **20**, 494207 (2008).
[25]A. Dewaele, J. H. Eggert, P. Loubeyre, and R. Le Toullec, Phys. Rev. B **67**, 094112 (2003).
[26]C.-S. Zha, R. J. Hemley, S. A. Gramsch, H.-k. Mao, and W. A. Bassett, J. Chem. Phys. **126**, 074506 (2007).
[27]J. C. Chervin, B. Canny, J. M. Besson, and Ph. Pruzan, Rev. Sci. Instrum. **66**(3), 2595 (1995).
[28]F. Datchi, P. Loubeyre, and R. LeToullec, Phys. Rev. B **61**, 6535 (2000).
[29]V. Giordano, F. Datchi, and A. Dewaele, J. Chem. Phys. **125**, 054504 (2006).
[30]H. K. Mao, J. Xu, and P. M. Bell, J. Geophys. Res. **91**(B5), 4673, doi:10.1029/JB091iB05p04673 (1986).
[31]D. R. Ragan, R. Gustacsen, and D. Schiferl, J. Appl. Phys. **72**(12), 5539 (1992).
[32]F. Datchi, A. Dewaele, P. Loubeyre, R. Letoullec, Y. Le Godec, and B. Canny, High Press. Res. **27**, 447 (2007).
[33]C. Sanchez-Valle, I. Daniel, B. Reynard, R. Abraham, and C. Goutaudier, J. Appl. Phys. **92**, 4349 (2002).
[34]C. H. Whitfield, E. M. Brody, and W. A. Bassett, Rev. Sci. Instrum. **47**(8), 942 (1976).
[35]S. V. Sinogeikin and J. D. Bass, Phys. Earth Planet. Inter. **120**, 43 (2000).
[36]C. Sanchez-Valle, C.-H. Chio, and G. D. Gatta, J. Appl. Phys. **108**, 093509 (2010).
[37]W. D. Wilson, J. Acoust. Soc. Am. **31**(8), 1067 (1959).
[38]A. H. Smith and A. W. Lawson, J. Chem. Phys. **22**, 351 (1954).
[39]G. Holton, J. Appl. Phys. **22**, 1407 (1951).
[40]P. L. M. Heydemann and J. C. Houck, J. Appl. Phys. **40**, 1609 (1969).
[41]F. Li, W. Cui, Z. He, T. Cui, J. Zhang, Q. Zhou, and G. Zou, J. Chem. Phys. **123**, 174511 (2005).
[42]M. Krich *et al.*, Phys. Rev. Lett. **89**, 125502 (2002).
[43]A. K. Soper and M. A. Ricci, Phys. Rev. Lett. **84**, 2881 (2000).
[44]T. Kawamoto, S. Ochiai, and H. Kagi, J. Chem. Phys. **120**, 5867 (2004).
[45]M. Saitta and F. Datchi, Phys. Rev. E **67**, 020201 (2003).
[46]F. Decremps, F. Datchi, and A. Polian, Ultrasonics **44**, e1495 (2006).
[47]D. Mantegazzi, C. Sanchez-Valle, E. Reusser, and T. Driesner, J. Chem. Phys. **137**, 224501 (2012).
[48]See supplementary material at http://dx.doi.org/10.1063/1.4789359 for a compilation of the thermodynamic properties of water to 673 K and 7 GPa derived from acoustic velocity measurements in the diamond anvil cell using Brillouin scattering spectroscopy.
[49]H. Shimizu, T. Kitagawa, and S. Sasaki, Phys. Rev. B **47**(17), 11567 (1993).
[50]F. Li *et al.*, J. Chem. Phys. **131**, 134502 (2009).
[51]M. Li *et al.*, J. Chem. Phys. **133**, 044503 (2010).
[52]A. H. Harvey, J. S. Gallagher, and J. M. H Levelt-Sengers, J. Phys. Chem. Ref. Data **27**, 761 (1998).
[53]L. Weiss, A. Tazibt, A. Tidu, and M. Aillerie, J. Chem. Phys. **136**, 124201 (2012).
[54]R. Setchell, J. Appl. Phys. **91**, 2833 (2002).
[55]K. Matsuishi, E. Gregoryanz, H.-k. Mao, and R. J. Hemley, J. Chem. Phys. **118**, 10683 (2003).
[56]T. Strassle *et al.*, Phys. Rev. Lett. **96**, 067801 (2006).